

1 ***Fermi* LAT Observation of Diffuse Gamma-Rays Produced Through**  
 2 **Interactions between Local Interstellar Matter and High Energy Cosmic Rays**

3 A. A. Abdo<sup>2,3</sup>, M. Ackermann<sup>4</sup>, M. Ajello<sup>4</sup>, W. B. Atwood<sup>5</sup>, M. Axelsson<sup>6,7</sup>, L. Baldini<sup>8</sup>,  
 4 J. Ballet<sup>9</sup>, G. Barbiellini<sup>10,11</sup>, D. Bastieri<sup>12,13</sup>, B. M. Baughman<sup>14</sup>, K. Bechtol<sup>4</sup>, R. Bellazzini<sup>8</sup>,  
 5 B. Berenji<sup>4</sup>, E. D. Bloom<sup>4</sup>, E. Bonamente<sup>15,16</sup>, A. W. Borgland<sup>4</sup>, J. Bregeon<sup>8</sup>, A. Brez<sup>8</sup>,  
 6 M. Brigida<sup>17,18</sup>, P. Bruel<sup>19</sup>, T. H. Burnett<sup>20</sup>, G. A. Caliandro<sup>17,18</sup>, R. A. Cameron<sup>4</sup>,  
 7 P. A. Caraveo<sup>21</sup>, P. Carlson<sup>22,7</sup>, J. M. Casandjian<sup>9</sup>, C. Cecchi<sup>15,16</sup>, Ö. Çelik<sup>23</sup>, A. Chekhtman<sup>2,24</sup>,  
 8 C. C. Cheung<sup>23</sup>, S. Ciprini<sup>15,16</sup>, R. Claus<sup>4</sup>, J. Cohen-Tanugi<sup>25</sup>, J. Conrad<sup>26,7,22,27</sup>, S. Cutini<sup>28</sup>,  
 9 C. D. Dermer<sup>2</sup>, A. de Angelis<sup>29</sup>, F. de Palma<sup>17,18</sup>, S. W. Digel<sup>4</sup>, E. do Couto e Silva<sup>4</sup>, P. S. Drell<sup>4</sup>,  
 10 R. Dubois<sup>4</sup>, D. Dumora<sup>30,31</sup>, C. Farnier<sup>25</sup>, C. Favuzzi<sup>17,18</sup>, S. J. Fegan<sup>19</sup>, W. B. Focke<sup>4</sup>,  
 11 M. Frailis<sup>29</sup>, Y. Fukazawa<sup>32</sup>, S. Funk<sup>4</sup>, P. Fusco<sup>17,18</sup>, F. Gargano<sup>18</sup>, D. Gasparrini<sup>28</sup>,  
 12 N. Gehrels<sup>23,33</sup>, S. Germani<sup>15,16</sup>, B. Giebels<sup>19</sup>, N. Giglietto<sup>17,18</sup>, F. Giordano<sup>17,18</sup>, T. Glanzman<sup>4</sup>,  
 13 G. Godfrey<sup>4</sup>, I. A. Grenier<sup>9</sup>, M.-H. Grondin<sup>30,31</sup>, J. E. Grove<sup>2</sup>, L. Guillemot<sup>30,31</sup>, S. Guiriec<sup>25,34</sup>,  
 14 Y. Hanabata<sup>32</sup>, A. K. Harding<sup>23</sup>, M. Hayashida<sup>4</sup>, E. Hays<sup>23</sup>, R. E. Hughes<sup>14</sup>, G. Jóhannesson<sup>4</sup>,  
 15 A. S. Johnson<sup>4</sup>, R. P. Johnson<sup>5</sup>, W. N. Johnson<sup>2</sup>, T. Kamae<sup>4</sup>, H. Katagiri<sup>32</sup>, N. Kawai<sup>35,36</sup>,  
 16 M. Kerr<sup>20</sup>, J. Knödseder<sup>37</sup>, M. L. Kocian<sup>4</sup>, F. Kuehn<sup>14</sup>, M. Kuss<sup>8</sup>, J. Lande<sup>4</sup>, L. Latronico<sup>8</sup>,  
 17 M. Lemoine-Goumard<sup>30,31</sup>, F. Longo<sup>38,10,11</sup>, F. Loparco<sup>17,18</sup>, B. Lott<sup>30,31</sup>, M. N. Lovellette<sup>2</sup>,  
 18 P. Lubrano<sup>15,16</sup>, A. Makeev<sup>2,24</sup>, M. N. Mazziotta<sup>18</sup>, J. E. McEnery<sup>23</sup>, C. Meurer<sup>26,7</sup>,  
 19 P. F. Michelson<sup>4</sup>, W. Mitthumsiri<sup>4</sup>, T. Mizuno<sup>32,1</sup>, A. A. Moiseev<sup>39,33</sup>, C. Monte<sup>17,18</sup>,  
 20 M. E. Monzani<sup>4</sup>, A. Morselli<sup>40</sup>, I. V. Moskalenko<sup>4</sup>, S. Murgia<sup>4</sup>, P. L. Nolan<sup>4</sup>, J. P. Norris<sup>41</sup>,  
 21 E. Nuss<sup>25</sup>, T. Ohsugi<sup>32</sup>, A. Okumura<sup>42</sup>, N. Omodei<sup>8</sup>, E. Orlando<sup>43</sup>, J. F. Ormes<sup>41</sup>, M. Ozaki<sup>44</sup>,  
 22 D. Paneque<sup>4</sup>, J. H. Panetta<sup>4</sup>, D. Parent<sup>30,31</sup>, M. Pepe<sup>15,16</sup>, M. Pesce-Rollins<sup>8</sup>, F. Piron<sup>25</sup>,  
 23 M. Pohl<sup>45</sup>, T. A. Porter<sup>5</sup>, S. Rainò<sup>17,18</sup>, R. Rando<sup>12,13</sup>, M. Razzano<sup>8</sup>, A. Reimer<sup>46,4</sup>,  
 24 O. Reimer<sup>46,4</sup>, T. Reposeur<sup>30,31</sup>, S. Ritz<sup>23</sup>, L. S. Rochester<sup>4</sup>, A. Y. Rodriguez<sup>47</sup>, F. Ryde<sup>22,7</sup>,  
 25 H. F.-W. Sadrozinski<sup>5</sup>, D. Sanchez<sup>19</sup>, A. Sander<sup>14</sup>, P. M. Saz Parkinson<sup>5</sup>, T. L. Schalk<sup>5</sup>,  
 26 A. Sellerholm<sup>26,7</sup>, C. Sgrò<sup>8</sup>, D. A. Smith<sup>30,31</sup>, P. D. Smith<sup>14</sup>, G. Spandre<sup>8</sup>, P. Spinelli<sup>17,18</sup>,  
 27 J.-L. Starck<sup>9</sup>, F. W. Stecker<sup>23</sup>, M. S. Strickman<sup>2</sup>, A. W. Strong<sup>43</sup>, D. J. Suson<sup>48</sup>, H. Tajima<sup>4</sup>,  
 28 H. Takahashi<sup>32</sup>, T. Takahashi<sup>44</sup>, T. Tanaka<sup>4</sup>, J. B. Thayer<sup>4</sup>, J. G. Thayer<sup>4</sup>, D. J. Thompson<sup>23</sup>,  
 29 L. Tibaldo<sup>12,13</sup>, D. F. Torres<sup>49,47</sup>, G. Tosti<sup>15,16</sup>, A. Tramacere<sup>4,50</sup>, Y. Uchiyama<sup>44,4</sup>, T. L. Usher<sup>4</sup>,  
 30 V. Vasileiou<sup>23,39,51</sup>, N. Vilchez<sup>37</sup>, V. Vitale<sup>40,52</sup>, A. P. Waite<sup>4</sup>, P. Wang<sup>4</sup>, B. L. Winer<sup>14</sup>,  
 31 K. S. Wood<sup>2</sup>, T. Ylinen<sup>22,53,7</sup>, M. Ziegler<sup>5</sup>

- 
- <sup>1</sup>Corresponding author: T. Mizuno, mizuno@hep01.hepl.hiroshima-u.ac.jp.
- <sup>2</sup>Space Science Division, Naval Research Laboratory, Washington, DC 20375, USA
- <sup>3</sup>National Research Council Research Associate, National Academy of Sciences, Washington, DC 20001, USA
- <sup>4</sup>W. W. Hansen Experimental Physics Laboratory, Kavli Institute for Particle Astrophysics and Cosmology, Department of Physics and SLAC National Accelerator Laboratory, Stanford University, Stanford, CA 94305, USA
- <sup>5</sup>Santa Cruz Institute for Particle Physics, Department of Physics and Department of Astronomy and Astrophysics, University of California at Santa Cruz, Santa Cruz, CA 95064, USA
- <sup>6</sup>Department of Astronomy, Stockholm University, SE-106 91 Stockholm, Sweden
- <sup>7</sup>The Oskar Klein Centre for Cosmo Particle Physics, AlbaNova, SE-106 91 Stockholm, Sweden
- <sup>8</sup>Istituto Nazionale di Fisica Nucleare, Sezione di Pisa, I-56127 Pisa, Italy
- <sup>9</sup>Laboratoire AIM, CEA-IRFU/CNRS/Université Paris Diderot, Service d’Astrophysique, CEA Saclay, 91191 Gif sur Yvette, France
- <sup>10</sup>Istituto Nazionale di Fisica Nucleare, Sezione di Trieste, I-34127 Trieste, Italy
- <sup>11</sup>Dipartimento di Fisica, Università di Trieste, I-34127 Trieste, Italy
- <sup>12</sup>Istituto Nazionale di Fisica Nucleare, Sezione di Padova, I-35131 Padova, Italy
- <sup>13</sup>Dipartimento di Fisica “G. Galilei”, Università di Padova, I-35131 Padova, Italy
- <sup>14</sup>Department of Physics, Center for Cosmology and Astro-Particle Physics, The Ohio State University, Columbus, OH 43210, USA
- <sup>15</sup>Istituto Nazionale di Fisica Nucleare, Sezione di Perugia, I-06123 Perugia, Italy
- <sup>16</sup>Dipartimento di Fisica, Università degli Studi di Perugia, I-06123 Perugia, Italy
- <sup>17</sup>Dipartimento di Fisica “M. Merlin” dell’Università e del Politecnico di Bari, I-70126 Bari, Italy
- <sup>18</sup>Istituto Nazionale di Fisica Nucleare, Sezione di Bari, 70126 Bari, Italy
- <sup>19</sup>Laboratoire Leprince-Ringuet, École polytechnique, CNRS/IN2P3, Palaiseau, France
- <sup>20</sup>Department of Physics, University of Washington, Seattle, WA 98195-1560, USA
- <sup>21</sup>INAF-Istituto di Astrofisica Spaziale e Fisica Cosmica, I-20133 Milano, Italy
- <sup>22</sup>Department of Physics, Royal Institute of Technology (KTH), AlbaNova, SE-106 91 Stockholm, Sweden
- <sup>23</sup>NASA Goddard Space Flight Center, Greenbelt, MD 20771, USA
- <sup>24</sup>George Mason University, Fairfax, VA 22030, USA
- <sup>25</sup>Laboratoire de Physique Théorique et Astroparticules, Université Montpellier 2, CNRS/IN2P3, Montpellier, France
- <sup>26</sup>Department of Physics, Stockholm University, AlbaNova, SE-106 91 Stockholm, Sweden
- <sup>27</sup>Royal Swedish Academy of Sciences Research Fellow, funded by a grant from the K. A. Wallenberg Foundation
- <sup>28</sup>Agenzia Spaziale Italiana (ASI) Science Data Center, I-00044 Frascati (Roma), Italy
- <sup>29</sup>Dipartimento di Fisica, Università di Udine and Istituto Nazionale di Fisica Nucleare, Sezione di Trieste, Gruppo

**ABSTRACT**

32

33

Observations by the Large Area Telescope (LAT) on the *Fermi* mission of diffuse  $\gamma$ -rays in a mid-latitude region in the third quadrant (Galactic longitude  $l$  from  $200^\circ$  to  $260^\circ$  and latitude  $|b|$  from  $22^\circ$  to  $60^\circ$ ) are reported. The region contains no known large molecular cloud and most of the atomic hydrogen is within 1 kpc of the solar system. The contributions of  $\gamma$ -ray point sources and inverse Compton scattering are

---

Collegato di Udine, I-33100 Udine, Italy

<sup>30</sup>Université de Bordeaux, Centre d'Études Nucléaires Bordeaux Gradignan, UMR 5797, Gradignan, 33175, France

<sup>31</sup>CNRS/IN2P3, Centre d'Études Nucléaires Bordeaux Gradignan, UMR 5797, Gradignan, 33175, France

<sup>32</sup>Department of Physical Sciences, Hiroshima University, Higashi-Hiroshima, Hiroshima 739-8526, Japan

<sup>33</sup>University of Maryland, College Park, MD 20742, USA

<sup>34</sup>University of Alabama in Huntsville, Huntsville, AL 35899, USA

<sup>35</sup>Department of Physics, Tokyo Institute of Technology, Meguro City, Tokyo 152-8551, Japan

<sup>36</sup>Cosmic Radiation Laboratory, Institute of Physical and Chemical Research (RIKEN), Wako, Saitama 351-0198, Japan

<sup>37</sup>Centre d'Étude Spatiale des Rayonnements, CNRS/UPS, BP 44346, F-30128 Toulouse Cedex 4, France

<sup>38</sup>Istituto Nazionale di Fisica Nucleare, Sezione di Trieste, and Università di Trieste, I-34127 Trieste, Italy

<sup>39</sup>Center for Research and Exploration in Space Science and Technology (CRESST), NASA Goddard Space Flight Center, Greenbelt, MD 20771, USA

<sup>40</sup>Istituto Nazionale di Fisica Nucleare, Sezione di Roma "Tor Vergata", I-00133 Roma, Italy

<sup>41</sup>Department of Physics and Astronomy, University of Denver, Denver, CO 80208, USA

<sup>42</sup>Department of Physics, Graduate School of Science, University of Tokyo, 7-3-1 Hongo, Bunkyo-ku, Tokyo 113-0033, Japan

<sup>43</sup>Max-Planck Institut für extraterrestrische Physik, 85748 Garching, Germany

<sup>44</sup>Institute of Space and Astronautical Science, JAXA, 3-1-1 Yoshinodai, Sagamihara, Kanagawa 229-8510, Japan

<sup>45</sup>Department of Physics and Astronomy, Iowa State University, Ames, IA 50011-3160, USA

<sup>46</sup>Institut für Astro- und Teilchenphysik, Leopold-Franzens-Universität Innsbruck, A-6020 Innsbruck, Austria

<sup>47</sup>Institut de Ciències de l'Espai (IEEC-CSIC), Campus UAB, 08193 Barcelona, Spain

<sup>48</sup>Department of Chemistry and Physics, Purdue University Calumet, Hammond, IN 46323-2094, USA

<sup>49</sup>Institució Catalana de Recerca i Estudis Avançats, Barcelona, Spain

<sup>50</sup>Consorzio Interuniversitario per la Fisica Spaziale (CIFS), I-10133 Torino, Italy

<sup>51</sup>University of Maryland, Baltimore County, Baltimore, MD 21250, USA

<sup>52</sup>Dipartimento di Fisica, Università di Roma "Tor Vergata", I-00133 Roma, Italy

<sup>53</sup>School of Pure and Applied Natural Sciences, University of Kalmar, SE-391 82 Kalmar, Sweden

estimated and subtracted. The residual  $\gamma$ -ray intensity exhibits a linear correlation with the atomic gas column density in energy from 100 MeV to 10 GeV. The measured integrated  $\gamma$ -ray emissivity is  $(1.63 \pm 0.05) \times 10^{-26}$  photons  $\text{s}^{-1} \text{sr}^{-1} \text{H-atom}^{-1}$  and  $(0.66 \pm 0.02) \times 10^{-26}$  photons  $\text{s}^{-1} \text{sr}^{-1} \text{H-atom}^{-1}$  above 100 MeV and above 300 MeV, respectively, with additional systematic error of  $\sim 10\%$ . The differential emissivity from 100 MeV to 10 GeV agrees with calculations based on cosmic ray spectra consistent with those directly measured, at the 10% level. The results obtained indicate that cosmic ray nuclei spectra within 1 kpc from the solar system in regions studied are close to the local interstellar spectra inferred from direct measurements at the Earth within  $\sim 10\%$ .

34 *Subject headings:* cosmic rays – diffuse radiation – gamma rays: observations

35

## 1. Introduction

36

The diffuse high energy  $\gamma$ -ray emission ( $E \geq 30$  MeV) has been interpreted to be a superposition of  $\gamma$ -rays produced via interactions between cosmic rays (CRs) and interstellar matter, inverse Compton (IC) scattering of interstellar soft photons off CR electrons, and the extragalactic diffuse  $\gamma$ -ray emission. The first component, if distinguished from the others, will enable using high-energy  $\gamma$ -ray observations for the study of the distribution of CRs and the interstellar medium. The distribution of neutral atomic hydrogen (HI) is traced by 21 cm line surveys and the molecular hydrogen distribution is derived indirectly using 2.6 mm line observations of carbon monoxide (CO). The total gas column density can also be traced indirectly from extinction and reddening by dust. Thus the spectrum and the flux of CRs can be obtained from sufficiently sensitive observations of high energy  $\gamma$ -rays. The observation of diffuse  $\gamma$ -rays away from the Galactic plane (Galactic latitude  $|b| \geq 10^\circ$ ) is suitable for studying local CRs, since diffuse  $\gamma$ -rays in such regions are less affected by contamination from strong point sources, and most of the gas along the line of sight is local. The SAS-2 (e.g., Fichtel, Simpson, & Thompson 1978) and COS-B observations (e.g., Lebrun et al. 1982) indicated a correlation between the  $\gamma$ -ray intensities and the total gas column densities at medium Galactic latitudes. Sreekumar et al. (1998) and Strong, Moskalenko, & Reimer (2004) showed a good correlation between the  $\gamma$ -ray intensities and model calculations in their analyses of the extragalactic diffuse emission observed by EGRET onboard the *Compton Gamma-Ray Observatory*. Despite these early studies, the flux and spectrum of local CRs deduced from  $\gamma$ -ray intensity remain uncertain, due to the possible contamination from unresolved point sources and uncertainties in modeling the IC contribution because of the large scale height of CR electrons and the reprocessing of the interstellar radiation by dust. Although CR nuclei in the vicinity of the solar system are thought to have spectral distributions and intensities similar to those measured at the Earth as reported by a number of  $\gamma$ -ray observations (e.g, Hunter et al. 1997; Digel et al. 2001), data above 1 GeV, which are crucial to distinguish CR nuclei spectra from that of CR electrons, have not been good enough due to the limited photon statistics and relatively limited energy coverage of these early missions.

37  
38  
39  
40  
41  
42  
43  
44  
45  
46  
47  
48  
49  
50  
51  
52  
53  
54  
55  
56  
57  
58  
59  
60  
61

62 The situation has improved significantly with the recent launch of the *Fermi* Gamma-ray Space  
 63 Telescope on 2008 June 11. The *Fermi* LAT (Large Area Telescope) has a sensitivity that is more  
 64 than an order of magnitude better than that of EGRET and enables resolving point sources and  
 65 studying the diffuse  $\gamma$ -rays with unprecedented sensitivity. Recent advances of a CR propagation  
 66 code GALPROP (e.g., Strong & Moskalenko 1998), which had been developed through comparisons  
 67 with the EGRET data, allow us to predict and subtract IC emission and correlate  $\gamma$ -ray emission  
 68 with interstellar matter more accurately.

69 In this paper, we present *Fermi* LAT observations of diffuse  $\gamma$ -rays in a mid-Galactic latitude  
 70 region in the third quadrant (Galactic longitude  $l$  from  $200^\circ$  to  $260^\circ$  and  $|b|$  from  $22^\circ$  to  $60^\circ$ ). As  
 71 discussed in the following sections, most of the gas along the line of sight is local, nearby on the  
 72 scale of the Milky Way. The contribution from IC emission is only about 10 % of the total diffuse  
 73 emission and the LAT has already resolved five times as many  $\gamma$ -ray point sources as previous  
 74 missions in this region. These facts enable us to evaluate the local CR flux and the spectrum with  
 75 small systematic uncertainty.

## 76 2. Observation and Data Reduction

77 The LAT is the main instrument of the *Fermi* Gamma-ray Space Telescope. It consists of  
 78  $4 \times 4$  modules (towers) built with tungsten foils and silicon microstrip detectors to measure the  
 79 arrival directions of incoming  $\gamma$ -rays, and a hodoscopic cesium iodide calorimeter to determine  
 80 the photon energies. They are surrounded by 89 segmented plastic scintillators serving as an  
 81 anticoincidence detector to reject charged particle events. Details of the LAT instrument and  
 82 pre-launch expectations of the performance can be found in Atwood et al. (2009). The excellent  
 83 sensitivity of the LAT is exemplified by initial publications such as Abdo et al. (2008).

84 Routine science operations with the LAT began on 2008 August 4. We have accumulated events  
 85 from 2008 August 4 to 2009 January 31 to study diffuse  $\gamma$ -rays. During this time interval the LAT  
 86 was operated in sky survey mode nearly all of the time; in this observing mode the LAT scans  
 87 the sky, obtaining complete sky coverage every two orbits and relatively uniform exposures over  
 88 time. We used the standard LAT analysis software, **ScienceTools**<sup>1</sup> version **v9r11**, and applied  
 89 the following event selection criteria: (1) events have the highest probability of being photons, i.e.,  
 90 they are categorized as so-called diffuse class (Atwood et al. 2009), (2) the reconstructed zenith  
 91 angles of the arrival direction of photons are selected to be less than  $105^\circ$ , in order to exclude  
 92 periods where the Earth enters the LAT field of view, and (3) the center of the LAT field of view  
 93 is within  $39^\circ$  from the zenith in order not to include the data taken in the pointed observation  
 94 mode, because it has increased contamination from Earth albedo  $\gamma$ -rays. We also eliminated the  
 95 period of time during which the LAT detected two bright GeV-emitting GRBs, i.e., GRB080916C

---

<sup>1</sup> available from the Fermi Science Support Center (<http://fermi.gsfc.nasa.gov/ssc/>)

96 (Abdo et al. 2009a) and GRB081024B (Omodei et al. 2008). We then generated count maps (using  
 97 **gtbin** in **ScienceTools**) and exposure maps (using **gtexpcube**) in 13 logarithmically-sliced energy  
 98 bins from 100 MeV to 9.05 GeV. A post-launch response function **P6\_V3\_DIFFUSE**, which was  
 99 developed to account for the  $\gamma$ -ray detection inefficiencies that are correlated with trigger rate,  
 100 was used in exposure calculations. These count and exposure maps were prepared in Cartesian  
 101 coordinates in  $0.5^\circ \times 0.5^\circ$  binning, and then transformed into HEALPIX<sup>2</sup> (Górski et al. 2005) equal  
 102 area sky maps of order=7. They are used below to correlate the  $\gamma$ -ray intensities with the column  
 103 densities of atomic gas along the line of sight; the  $\gamma$ -ray intensity is calculated as the ratio of the  
 104 counts and the exposures for each energy bin.

### 105 3. Data Analysis

#### 106 3.1. Subtraction of Inverse Compton and Point Sources

107 To distinguish  $\gamma$ -rays produced in the interstellar medium from others, we referred to the GAL-  
 108 PROP prediction of IC emission and an LAT source list for 6 month data<sup>3</sup>. This list was produced  
 109 using a similar procedure used to obtain the LAT Bright Source List described by Abdo et al.  
 110 (2009b). It covers the same period of time as that of our data set and contains 740 point sources  
 111 with significance more than  $5\sigma$ . We adopted positions and spectral parameters from this list (single  
 112 power-law model in 100 MeV–100 GeV) to estimate and subtract the photons from point sources to  
 113 diffuse  $\gamma$ -ray emission. GALPROP (e.g., Strong & Moskalenko 1998) is a set of programs to solve  
 114 the CR transport equation within our Galaxy and predict the  $\gamma$ -ray emission produced via inter-  
 115 actions of CRs with interstellar matter (nucleon-nucleon interaction and electron bremsstrahlung)  
 116 and soft photons (IC scattering). IC emission is calculated from the distribution of (propagated)  
 117 electrons and the interstellar radiation fields developed by Moskalenko, Porter, & Strong (2006).  
 118 Here we adopted the IC model map with version **54.5gXvarh7S**<sup>4</sup>, which was used in another  
 119 *Fermi* LAT paper to study the diffuse  $\gamma$ -ray emission in  $10^\circ \leq |b| \leq 20^\circ$  (Abdo et al. 2009d). The  
 120 CR electron spectrum is adjusted to agree with the directly-measured pre-Fermi spectrum in this  
 121 GALPROP model. In order to minimize the uncertainty of the contribution from IC emission on  
 122 the diffuse  $\gamma$ -ray spectrum, we selected sky regions away from the Galactic center; the lower CR  
 123 electron fluxes and interstellar radiation field will result in dimmer IC emission than that toward  
 124 the Galactic center. We chose the third quadrant, Galactic longitude  $l$  from  $200^\circ$  to  $260^\circ$  and the  
 125 Galactic latitude  $b$  from  $-60^\circ$  to  $-22^\circ$  and from  $22^\circ$  to  $60^\circ$ . The region is free of known large  
 126 molecular clouds; Orion molecular clouds (Orion A and Orion B) and Monoceros molecular cloud  
 127 complexes are located in the region  $l$  from  $200^\circ$  to  $220^\circ$  and  $b$  from  $-10^\circ$  to  $-20^\circ$ , and the Tau-

---

<sup>2</sup><http://healpix.jpl.nasa.gov>

<sup>3</sup>internally available to the LAT team

<sup>4</sup> The GALPROP galdef ID of this version is available at the website <http://galprop.stanford.edu>

128 rus/Perseus molecular clouds are in  $l$  from  $150^\circ$  to  $185^\circ$  (e.g., Dame, Hartmann, & Thaddeus 2001;  
 129 Digel et al. 1999; Digel & Grenier 2001). Therefore the region described is suitable for correlating  
 130 the  $\gamma$ -ray intensities with the local atomic-gas column densities.

131 In Figure 1, we show  $\gamma$ -ray count maps above 100 MeV. There are 52 sources in the LAT  
 132 6 month source list in our region of interest, more than five times as many sources in the third  
 133 EGRET catalog (Hartman et al. 1999) in this region (nine sources). The diffuse  $\gamma$ -ray spectrum,  
 134 after masking sources with circular regions of  $1^\circ$  radius, is shown in Figure 2. Atomic hydrogen  
 135 column density maps of the same region (see Section 3.2 for details) are given in Figure 3. In  
 136 Figure 2 and figures shown hereafter (Figures 4–6), the  $\gamma$ -ray intensities or CR fluxes multiplied by  
 137  $E^2$  (where  $E$  is the center of each energy bin in logarithmic scale) are presented. Also presented in  
 138 Figure 2 is the contribution from IC emission predicted by GALPROP, and the spillover from point  
 139 sources outside the mask regions estimated (using `gtmodel`) by the spectral parameters given in  
 140 the source list. Both the flux of estimated IC emission and the residual point source contribution are  
 141 less than 15 % of the total diffuse emission above 100 MeV. We thus conclude that the uncertainty  
 142 due to the IC and point source contributions is negligible after we subtract them from  $\gamma$ -ray data.  
 143 Hereafter we analyze diffuse emission after masking point sources and subtracting IC emission and  
 144 the residual contributions from point sources.

### 145 3.2. Atomic Hydrogen Map

146 Column densities  $N(\text{HI})$  of atomic hydrogen gas were calculated from existing radio surveys  
 147 of the 21 cm line of HI. We used the Leiden/Argentine/Bonn (LAB) Survey which merges the  
 148 Leiden/Dwingeloo Survey (Hartmann & Burton 1997) with the Instituto Argentino de Radioas-  
 149 tronomia Survey (Arnal et al. 2000; Bajaja et al. 2005) and covers the entire sky. We applied an  
 150 optical depth correction under the assumption of a uniform spin temperature of 125 K and the cos-  
 151 mic microwave background intensity at 1420 MHz of 2.66 K (e.g., Hunter et al. 1994). The derived  
 152 HI column density maps of our region of interest are shown in Figure 3. Although major CO sur-  
 153 veys such as the one by Dame, Hartmann, & Thaddeus (2001) do not cover the region we analyzed,  
 154 no large molecular cloud is known there and the molecular gas contribution is expected to be small  
 155 due to the moderately high Galactic latitude. See the discussion by Dame, Hartmann, & Thaddeus  
 156 (2001) for the completeness of their survey. Hereafter we assume that all the gas is in atomic form  
 157 and traced by 21 cm radio surveys. Column densities of HI in our region range from  $1 \times 10^{20} \text{ cm}^{-2}$   
 158 up to  $18 \times 10^{20} \text{ cm}^{-2}$  and the optical depth correction is rather small; the increase of the col-  
 159 umn densities from those for the optically thin case (infinite spin temperature) is  $\leq 10$  % in most  
 160 directions. On the assumption of a Galactic rotation curve by Clemens (1985) for the case of  
 161  $R_0 = 8.5 \text{ kpc}$  and  $\theta_0 = 220 \text{ km s}^{-1}$  (where  $R_0$  and  $\theta_0$  are the Galactocentric radius and the orbital  
 162 velocity of the local group of stars, respectively), we infer that, in almost every direction in our  
 163 region, more than 80 % of the HI along the line of sight is within 1 kpc of the solar circle. Further-  
 164 more, by referring to the vertical density distribution of HI given by Dickey & Lockman (1990),

165 we can conclude that more than 85 % of atomic gas in the line of sight is within 1 kpc of the solar  
 166 system for  $|b| \geq 22^\circ$ .

### 167 3.3. Correlation of $\gamma$ -ray Intensities and Gas Column Densities

168 The LAT point-spread function (PSF) strongly depends on the photon energy (e.g., Atwood et al.  
 169 2009) and the energy dependence of the angular size needs to be taken into account in data analy-  
 170 sis. We convolved the map of HI column densities obtained as described in Section 3.2 using the  
 171 GaDGET package (Ackermann et al. 2008) with the LAT PSF for each of our energy bins; in the  
 172 convolution we used the all sky map to take account of the contribution from outside the region for  
 173 the analysis. Since the typical angular size of the variation of column densities is a few degrees (see  
 174 Figure 3), only maps for the lowest energy bands (less than a few hundred MeV) are noticeably  
 175 smeared.

176 The  $\gamma$ -ray intensities, after masking point sources with  $1^\circ$  circular regions and subtracting the  
 177 IC emission and the residual point source contributions, are correlated with the HI column densities  
 178 in each energy band. Both the  $\gamma$ -ray intensity map and the HI column density map were prepared  
 179 in HEALPix equal area sky maps of order=7, whose pixel size in solid angle is  $6.39 \times 10^{-5}$  steradian  
 180 and is close to that of  $0.5 \times 0.5 \text{ deg}^2$ . We found a linear relationship between  $N(\text{HI})$  and residual  
 181  $\gamma$ -ray intensities for energies from 100 MeV to 10 GeV. Above 10 GeV the correlation is limited  
 182 by photon statistics. Figure 4 shows the correlation between  $\gamma$ -ray intensities and the HI column  
 183 densities for four representative energy bands. The linear correlation indicates that point source  
 184 contributions are successfully subtracted and residual  $\gamma$ -rays mostly originate from interstellar  
 185 atomic gas through interactions with CRs, plus isotropic diffuse component (extragalactic diffuse  
 186  $\gamma$ -rays, the residual particle background, and a possible residual of IC emission).

187 By fitting the correlation in each energy band with a linear function using a  $\chi^2$  minimization,  
 188 we obtained the intensity of the isotropic diffuse component and the emissivity of atomic gas as  
 189 the offset and the slope, respectively, as summarized in Table 1. Making the mask region larger, to  
 190  $3^\circ$  radius, gives consistent fit parameters within statistical errors, confirming that the contribution  
 191 of point sources is well modeled and subtracted. The obtained isotropic diffuse component (offset  
 192 column in Table 1) agrees within 10–20 % with the "Isotropic" component given in Abdo et al.  
 193 (2009d) which investigates the medium-latitude diffuse emission. We note that the isotropic diffuse  
 194 components obtained here and in Abdo et al. (2009d) include the residual background and thus  
 195 should be regarded as an upper limit of the true extragalactic diffuse  $\gamma$ -ray emission. We also note  
 196 that the adopted IC model affects the spectral shape and the intensity of our isotropic component,  
 197 whereas it does not affect the emissivity significantly; modifying the IC emission by  $\pm 50$  % changes  
 198 the offsets by 6 %–7 %, but alters the slopes less than 3 % except the lowest two energy bands. A  
 199 detailed study of the extragalactic diffuse emission and the residual background using data for a  
 200 larger sky area is underway and will be published elsewhere (A. A. Abdo et al. 2009, in preparation).



201 So far, we have been neglecting the contribution from CR interactions with ionized hydrogen  
 202 (H II). The low-density ionized gas is unobservable, but can be inferred from dispersion measures  
 203 of pulsar signals in the radio band. According to the model of Cordes & Lazio (2002), in the region  
 204 we are studying,  $N(\text{H II})$  is only  $(1\text{--}2) \times 10^{20} \text{ cm}^{-2}$  and fairly smooth. We thus conclude that the  
 205 contribution from ionized gas does not affect the obtained emissivity significantly.

#### 206 4. Discussion

207 With the approach described in Section 3, we succeeded in decoupling diffuse  $\gamma$ -rays related  
 208 to the local atomic gas from point sources, the IC emission, and the isotropic diffuse compo-  
 209 nent. The derived differential  $\gamma$ -ray emissivity from the local atomic gas is given in Figure 5.  
 210 The systematic uncertainty of the effective area of the response we used (**P6\_V3\_DIFFUSE**)  
 211 is estimated to be 10 %, 5 % and 20 % at 100 MeV, 560 MeV, and 10 GeV, respectively, and  
 212 depend on the energy linearly in a logarithmic scale. This systematic uncertainty is compara-  
 213 ble with the statistical error, and is indicated by the shaded area in the figure. The integral  
 214 emissivity above 100 MeV and 300 MeV is  $(1.63 \pm 0.05) \times 10^{-26} \text{ photons s}^{-1} \text{ sr}^{-1} \text{ H-atom}^{-1}$  and  
 215  $(0.66 \pm 0.02) \times 10^{-26} \text{ photons s}^{-1} \text{ sr}^{-1} \text{ H-atom}^{-1}$ , respectively, with an additional systematic un-  
 216 certainty of  $\sim 10$  %. These values can be compared with those reported by early measurements.  
 217 SAS-2 (Fichtel, Simpson, & Thompson 1978) obtained about  $3 \times 10^{-26} \text{ photons s}^{-1} \text{ sr}^{-1} \text{ H-atom}^{-1}$   
 218 and COS-B (Lebrun et al. 1982) reported  $(1.67 \pm 0.24) \times 10^{-26} \text{ photons s}^{-1} \text{ sr}^{-1} \text{ H-atom}^{-1}$  above  
 219 100 MeV. The EGRET analysis of various directions toward large molecular clouds (Digel et al.  
 220 2001) gives  $(1.65\text{--}2.4) \times 10^{-26} \text{ photons s}^{-1} \text{ sr}^{-1} \text{ H-atom}^{-1}$  and  $(0.71\text{--}1.0) \times 10^{-26} \text{ photons s}^{-1} \text{ sr}^{-1} \text{ H-atom}^{-1}$   
 221 above 100 MeV and 300 MeV, respectively. While most of these early measurements are consistent  
 222 with the LAT data, the emissivity obtained by the LAT is much improved in photon statistics and  
 223 energy range.

224 We can give constraints on the local CR spectrum by comparing the obtained emissivity with  
 225 the model calculation of interactions between CRs and interstellar matter. Many evaluations of  
 226 the  $\gamma$ -ray production due to CR interactions in the interstellar medium have been made, including  
 227 Stecker (1973, 1989), Dermer (1986a,b), Bertsch et al. (1993), Mori (1997), Kamae et al. (2006)  
 228 and Huang et al. (2007). In the calculation of neutral pion production and decay  $\gamma$ -rays, most  
 229 authors have computed the  $\gamma$ -ray flux produced through interactions of high-energy CR protons  
 230 with proton targets. The effects of heavy nuclei in both CRs and the target matter are usually  
 231 taken into account as a so-called nuclear enhancement factor ( $\epsilon_M$ ) to multiply the proton-proton  
 232  $\gamma$ -ray yield. Although the predicted  $\gamma$ -ray spectra from proton-proton interactions assuming the  
 233 same CR proton spectrum agree well ( $\leq 10$  %) among these works (e.g., Kamae et al. 2006), the  
 234 nuclear enhancement factors differ by up to  $\sim 30$  %; the factors range from 1.45 to 1.80–2.0 as  
 235 compiled by Mori (2009). Among them, Dermer (1986a,b) gives the lowest  $\epsilon_M$  of 1.45, and Mori  
 236 (2009) gives the highest  $\epsilon_M$  of 1.84 at the CR proton kinetic energy of 10 GeV. His higher value  
 237 of  $\epsilon_M$  is attributed to the adoption of recent CR spectral formulae by Honda et al. (2004) and the

238 inclusion of nuclei heavier than He in both the interstellar medium and the CR spectra. We thus  
 239 regard  $\epsilon_M$  by Mori (2009) as the most reliable.

240 In calculating the neutral pion production, we used the proton-proton interaction formalism by  
 241 Kamae et al. (2006). They gave parameterized formulae of the  $\pi^0$  inclusive cross section and decay  
 242  $\gamma$ -ray spectra for arbitrary proton kinetic energies from 0.488 GeV to 512 TeV. We adopted the  
 243 proton local interstellar spectrum (LIS) from the GALPROP model with **54\_5gXvarh7S** and cal-  
 244 culated the  $\gamma$ -ray spectrum from nucleon-nucleon interactions using formulae given by Kamae et al.  
 245 (2006) under the assumption of the nuclear enhancement factor to be 1.84 as a representative value  
 246 of those by Mori (2009). In order to calculate the electron bremsstrahlung, we fully utilized GAL-  
 247 PROP which calculates the  $\gamma$ -ray spectrum using a formalism by Koch & Motz (1959) as explained  
 248 by Strong, Moskalenko, & Reimer (2000).

249 The predicted emissivity at the solar sytem (Galactocentric radius  $R = 8.5$  kpc and the height  
 250 from the Galactic plane  $z = 0$  kpc) is compared with our LAT measurement in Figure 5, and  
 251 the LIS of proton, electron and positron used in this model calculation is presented in Figure 6.  
 252 Also shown is a compilation of some measurements of proton and electron spectra at the Earth.  
 253 The proton and electron model spectra follow the observed ones above a few tens of GeV; below  
 254 this energy the solar wind lowers the observed fluxes. We note that the CR electron spectrum  
 255 measured by the LAT is somewhat harder than the GALPROP model (Abdo et al. 2009c), but  
 256 the effect on our analysis is negligible. We also note that the bremsstrahlung at around 100 MeV  
 257 has comparable contributions from both primary electrons and secondary electrons/positrons, as  
 258 discussed by Porter et al. (2008). Their contributions are included in the computed spectrum shown  
 259 in Figure 5.

260 The true LIS is somewhat uncertain due to solar activity. To model this solar modulation  
 261 effect on the CR spectrum, the formula by Gleeson & Axford (1968) generally has been used, in  
 262 which a single parameter  $\phi$  is introduced. The proton LIS we adopted reproduces the observations  
 263 at the Earth with  $\phi = 450$  MV as shown in Figure 6. The same data can also be reproduced by  
 264 a different formula of the LIS (dotted blue line) with  $\phi = 600$  MV as described by Shikaze et al.  
 265 (2007). We thus regard the difference between two models as representing the uncertainty of the  
 266 LIS; they agree well ( $\leq 10\%$ ) above 10 GeV and differ by  $\sim 20\%$  at about 3 GeV. This affects the  
 267 calculated emissivity by  $\sim 20\%$  and  $\leq 10\%$  at about 100 MeV and above 1 GeV, respectively (e.g.,  
 268 Mori 1997). We note that the LIS we adopted better reproduces the observed proton spectrum  
 269 above 20 GeV. Although the true LIS below 1 GeV is highly uncertain, these CRs do not contribute  
 270 to the  $\gamma$ -ray emissivity above 100 MeV significantly.

271 As shown in Figure 5, the emissivity measured by the LAT agrees with the prediction from  
 272 the assumed LIS and the recent estimate of  $\epsilon_M$  at the 10 % level, which is comparable with the  
 273 statistical error and the current systematic uncertainty of the LAT response. For reference, we  
 274 also show the  $\gamma$ -ray emissivity model obtained with the lowest  $\epsilon_M$  (among references in Mori 2009)  
 275 of 1.45 that gives a predicted emissivity lower than that observed in 100 MeV–10 GeV. Since the

276 nucleon-nucleon component is dominant in the emissivity spectrum especially above 1 GeV, the  
277 observed agreement between the LAT data and the model calculation (with the latest estimate of  
278  $\epsilon_M$ ) indicates that CR nuclei in the vicinity of the solar system in regions observed have spectral  
279 distributions and intensities close to those of the LIS inferred from measurements at the Earth  
280 within  $\sim 10\%$ . Although the constraint is rather weak, the agreement down to 100 MeV also  
281 suggests that highly uncertain low-energy (below a few hundred MeV) CR electron and positron  
282 spectra are compatible with our assumption (GALPROP model with **54.5gXvarh7S**) shown in  
283 Figure 6.

## 284 5. Summary and Conclusions

285 We report the observation of diffuse  $\gamma$ -rays in a mid-latitude region in the third quadrant using  
286 data from the first six months of *Fermi* LAT science observations. The region is away from the  
287 Galactic plane and the Galactic center, and contains no known large molecular cloud. Most of the  
288 atomic hydrogen is within 1 kpc of the solar system, and thus the region is suitable for studying the  
289  $\gamma$ -ray emissivity of the local atomic gas and CR spectra in the neighborhood of the solar system.  
290 Thanks to the excellent performance of the LAT and recent developments of the CR propagation  
291 code and the interstellar radiation field model in GALPROP, we reliably estimated and subtracted  
292 the contribution from point sources and IC emission. The residual  $\gamma$ -ray intensities exhibit a  
293 linear relationship with the atomic gas column densities from 100 MeV to 10 GeV, indicating that  
294 non-isotropic  $\gamma$ -rays are produced through interactions of CRs with interstellar atomic gas. The  
295 measurement of the emissivity of local atomic hydrogen has already surpassed those by past missions  
296 in photon statistics and the energy range. It agrees with the prediction from CR spectra assumed,  
297 indicating that the CR nuclei spectra in the vicinity of the solar system in regions analyzed are  
298 close to the LIS inferred from direct measurements at the Earth within  $\sim 10\%$ . Low energy CR  
299 electron/positron spectra are suggested to be compatible with our assumption.

300 The *Fermi* LAT Collaboration acknowledges generous ongoing support from a number of  
301 agencies and institutes that have supported both the development and the operation of the LAT as  
302 well as scientific data analysis. These include the National Aeronautics and Space Administration  
303 and the Department of Energy in the United States, the Commissariat à l’Energie Atomique and  
304 the Centre National de la Recherche Scientifique / Institut National de Physique Nucléaire et de  
305 Physique des Particules in France, the Agenzia Spaziale Italiana and the Istituto Nazionale di Fisica  
306 Nucleare in Italy, the Ministry of Education, Culture, Sports, Science and Technology (MEXT),  
307 High Energy Accelerator Research Organization (KEK) and Japan Aerospace Exploration Agency  
308 (JAXA) in Japan, and the Swedish Research Council and the Swedish National Space Board in  
309 Sweden. Additional support for science analysis during the operations phase from the following  
310 agencies is also gratefully acknowledged: the Istituto Nazionale di Astrofisica in Italy and the  
311 K. A. Wallenberg Foundation in Sweden.

312 Some of the results in this paper have been derived using the HEALPix (Górski et al. 2005)  
313 package.

## 314 REFERENCES

- 315 Abdo, A. A. et al. 2008, *Science*, 322, 1218
- 316 Abdo, A. A. et al. 2009a, *Science*, 323, 1688
- 317 Abdo, A. A. et al. 2009b, *ApJS*, 183, 46
- 318 Abdo, A. A. et al. 2009c, *Phys. Rev. Lett.*, 102, 181101
- 319 Abdo, A. A. et al. 2009d, *Phys. Rev. Lett.*, submitted; see also Porter et al. (arXiv:0907.0294)
- 320 Ackermann, M., Jóhannesson, G., Digel, S., Moskalenko, I. V., Porter, A., Reimer, O., & Strong, A.  
321 2008, in *AIP Conf. Proc.* 1085, *High Energy Gamma-ray Astronomy*, ed. F. A. Aharonian,  
322 W. Hofmann, & F. Rieger (New York: AIP), 763
- 323 Alcaraz, J. et al. 2000a, *Phys. Lett. B.*, 472, 215
- 324 Alcaraz, J. et al. 2000b, *Phys. Lett. B.*, 484, 10
- 325 Arnal, E. M., Bajaja, E., Larrarte, J. J., Morras, E., & Pöppel, W. G. L. 2000, *A&AS*, 142, 35
- 326 Atwood, W. B. et al. 2009, *ApJ*, 697, 1071
- 327 Bajaja, E., Arnal, E. M., Larrarte, J. J., Morras, R., Pöppel, W. G. L., & Kalberla, P. M. W. 2005,  
328 *A&A*, 440, 767
- 329 Barwick, S. W. et al. 1998, *ApJ*, 498, 779
- 330 Bertsch, D. L., Dame, T. M., Fichtel, C. E., Hunter, S. D., Sreekumar, P., Stacy, J. G., & Thaddeus,  
331 P. 1993, *ApJ*, 416, 587
- 332 Clemens, D. P. 1985, *ApJ*, 295, 422
- 333 Cordes, J. M., & Lazio, T. J. W. 2002, arXiv:astro-ph/0207156
- 334 Dame, T. M., Hartmann, D., & Thaddeus, P. 2001, *ApJ*, 547, 792
- 335 Dermer, C. D. 1986a, *ApJ*, 307, 47
- 336 Dermer, C. D. 1986b, *A&A*, 157, 223
- 337 Dickey, J. M., & Lockman, F. J. 1990, *ARA&A*, 28, 215

- 338 Digel, S. W., & Grenier, A. 2001, in AIP Conf. Proc. 587, Gamma-Ray Astrophysics, ed. S. Ritz,  
339 N. Gehrels, & C. R. Shrader (Melville, NY: AIP), 538
- 340 Digel, S. W., Aprile, E., Hunter, S. D., Mukherjee, R., Xu, F. 1999, ApJ, 520, 196
- 341 Digel, S. W., Grenier, I. A., Hunter, S. D., Dame, T. M., & Thaddeus, P. 2001, ApJ, 555, 12
- 342 Fichtel, C. E., Simpson, G. A., & Thompson, D. J. 1978, ApJ, 222, 833
- 343 Gleeson, N., & Axford, W. I. 1968, ApJ, 154, 1011
- 344 Górski, K. M., Hivon, E., Banday, A. J., Wandelt, B. D., Hansen, F. K., Reinecke, B., & Bartel-  
345 mann, B. 2005, ApJ, 622, 759
- 346 Hartman, R. C. et al. 1999, ApJS, 123, 79
- 347 Hartmann, D., & Burton, W. B. 1997, Atlas of Galactic Neutral Hydrogen, (Cambridge, UK:  
348 Cambridge Univ. Press)
- 349 Honda, M., Kajita, T., Kasahara, K., & Midorikawa, S. 2004, Phys. Rev., D70, 043008
- 350 Huang, C. -Y., Park., S. -E., Pohl, M., & Daniels, C. D. 2007, Astroparticle Physics, 27, 429
- 351 Hunter, S. D., Digel, S. W., de Geus, E. J. & Kanbash, G. 1994, ApJ, 436, 216
- 352 Hunter, S. D. et al. 1997, ApJ, 481, 205
- 353 Kamae, T., Karlsson, N., Mizuno, T., Abe, T., & Koi, T. 2006, ApJ, 647, 692
- 354 Koch, H. W., & Motz, J. W. 1959, Rev. Mod. Phys., 31, 920
- 355 Lebrun, F. et al. 1982, A&A, 107, 390
- 356 Mori, M. 1997, ApJ, 478, 225
- 357 Mori, M. 2009, Astroparticle Physics, 31, 341
- 358 Moskalenko, I. V., Porter, T. A., & Strong, A. W., 2006, ApJ, 640, 155
- 359 Omodei, N. et al. 2008, GRB Coordinates Network, 8407
- 360 Porter, T., Moskalenko, I. V., Strong, A. W., Orlando, E., & Bouchet, L., 2008, ApJ, 682, 400
- 361 Sanuki, T. et al. 2000, ApJ, 545, 1135
- 362 Shikaze, Y. et al. 2007 Astroparticle Physics, 28, 154
- 363 Sreekumar, P. et al. 1998, ApJ, 494, 523
- 364 Stecker, F. W. 1973, ApJ, 185, 499

- 365 Stecker, F. W. 1989, in *Cosmic Gamma Rays, Neutrinos and Related Astrophysics*, ed. by M. M.  
366 Shapiro and J. P. Wefel (Dordrecht; Kluwer), 85
- 367 Strong, A. W., & Moskalenko, I. V. 1998, *ApJ*, 509, 212
- 368 Strong, A. W., Moskalenko, I. V., & Reimer, O. 2000, *ApJ*, 537, 763
- 369 Strong, A. W., Moskalenko, I. V., & Reimer, O. 2004, *ApJ*, 613, 956

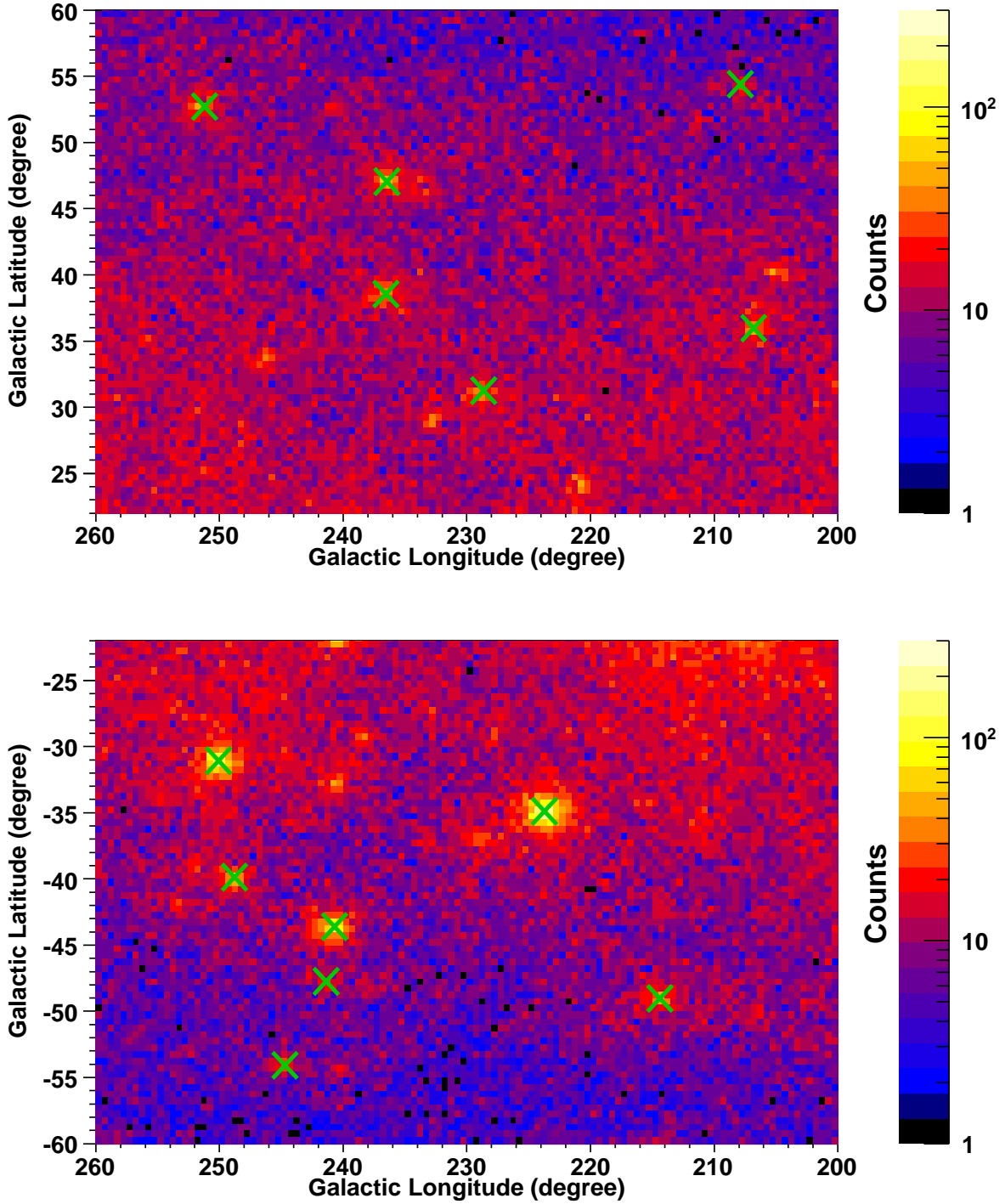


Fig. 1.— *Fermi* LAT  $\gamma$ -ray count maps ( $E \geq 100$  MeV) of regions we analyzed. Maps are in Cartesian projection with  $0.5^\circ \times 0.5^\circ$  binning. The north and the south regions are shown in the upper panel and the lower panel, respectively. In these regions there are 52 sources in the LAT 6 month source list, of which 13 sources (indicated by green crosses) are included in the LAT Bright Source List (Abdo et al. 2009b).

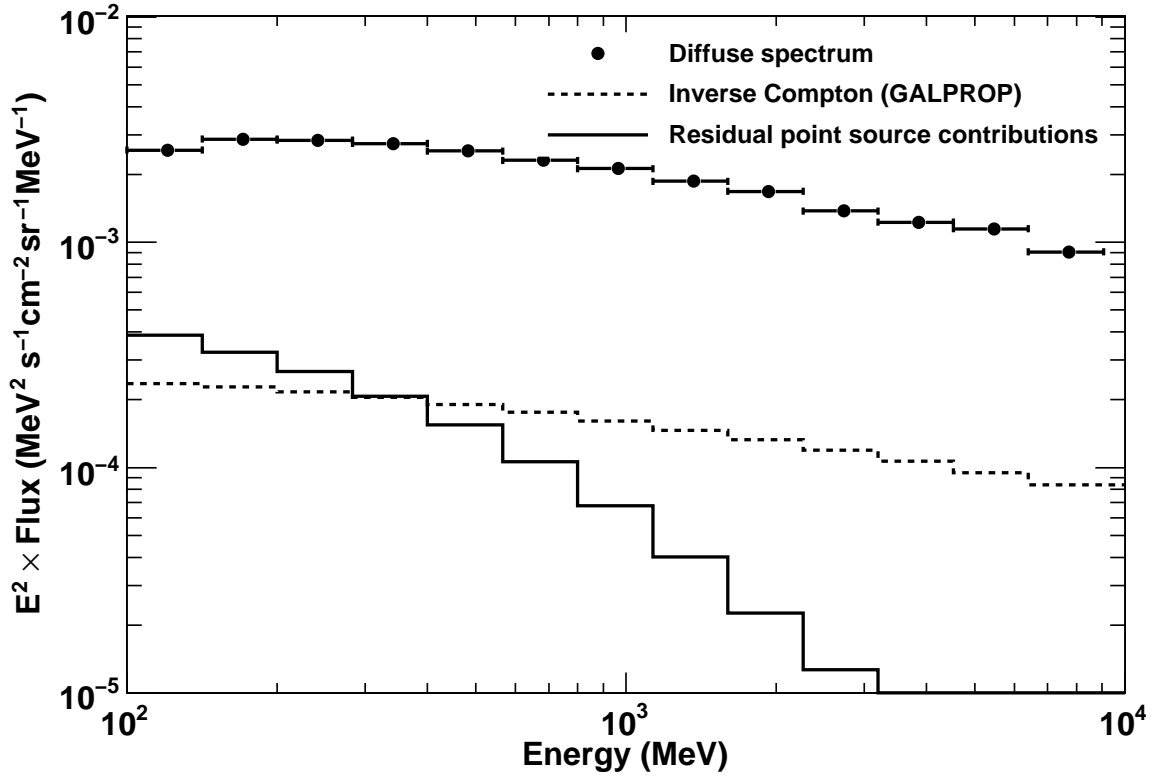


Fig. 2.— Diffuse  $\gamma$ -ray spectrum in regions analyzed ( $l$  from  $200^\circ$  to  $260^\circ$  and  $|b|$  from  $22^\circ$  to  $60^\circ$ ) after masking point sources with circular regions of  $1^\circ$  radius. IC emission predicted by GALPROP (54.5gXvarh7S) and the residual point source contributions estimated from spectral parameters given in the LAT 6 month source list are shown by dotted and solid histograms, respectively. The horizontal and vertical error bars indicate the energy ranges and  $1\sigma$  statistical errors, respectively.



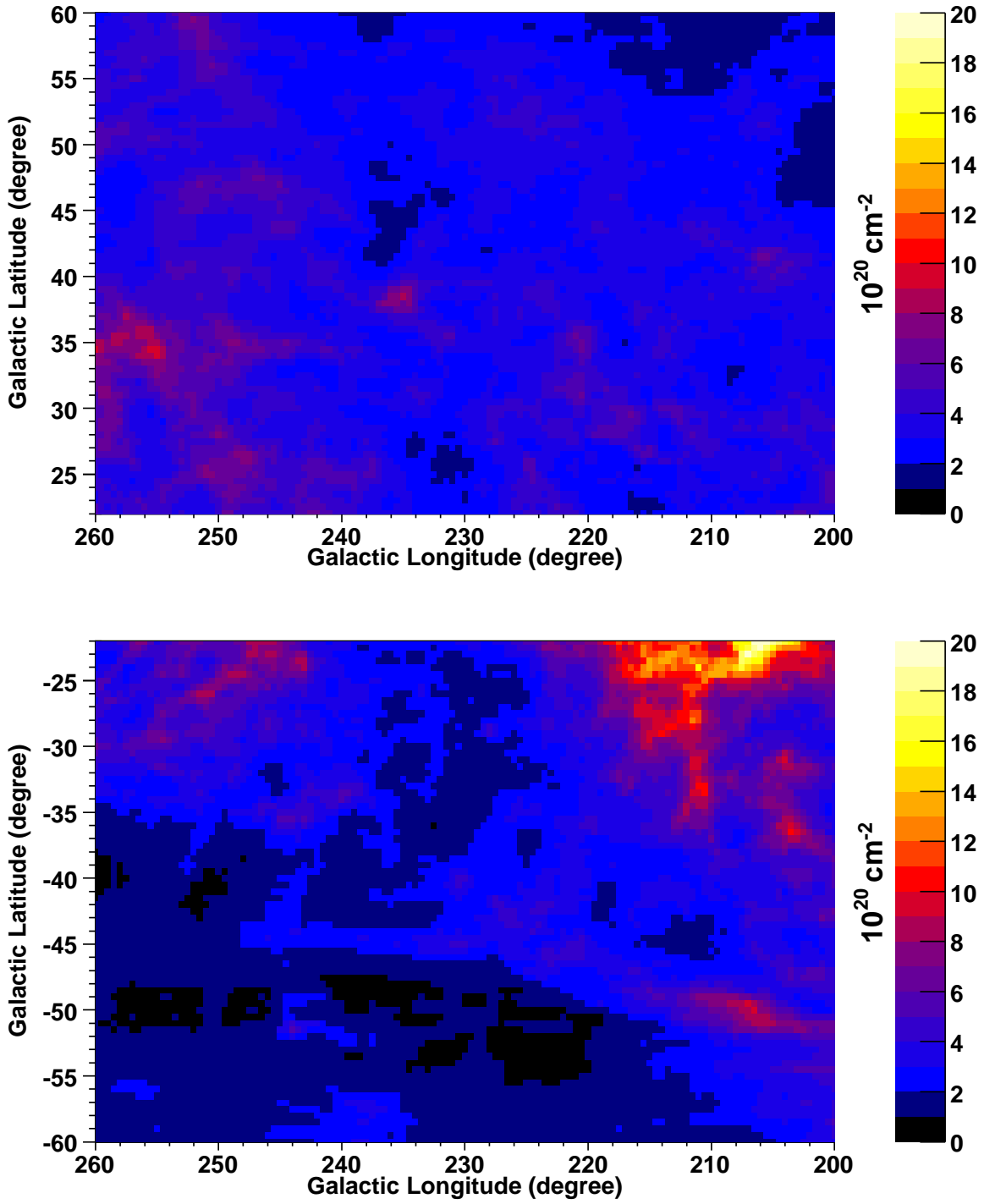


Fig. 3.— Column density maps of atomic hydrogen derived from the LAB survey under the assumption of a uniform spin temperature of 125 K.

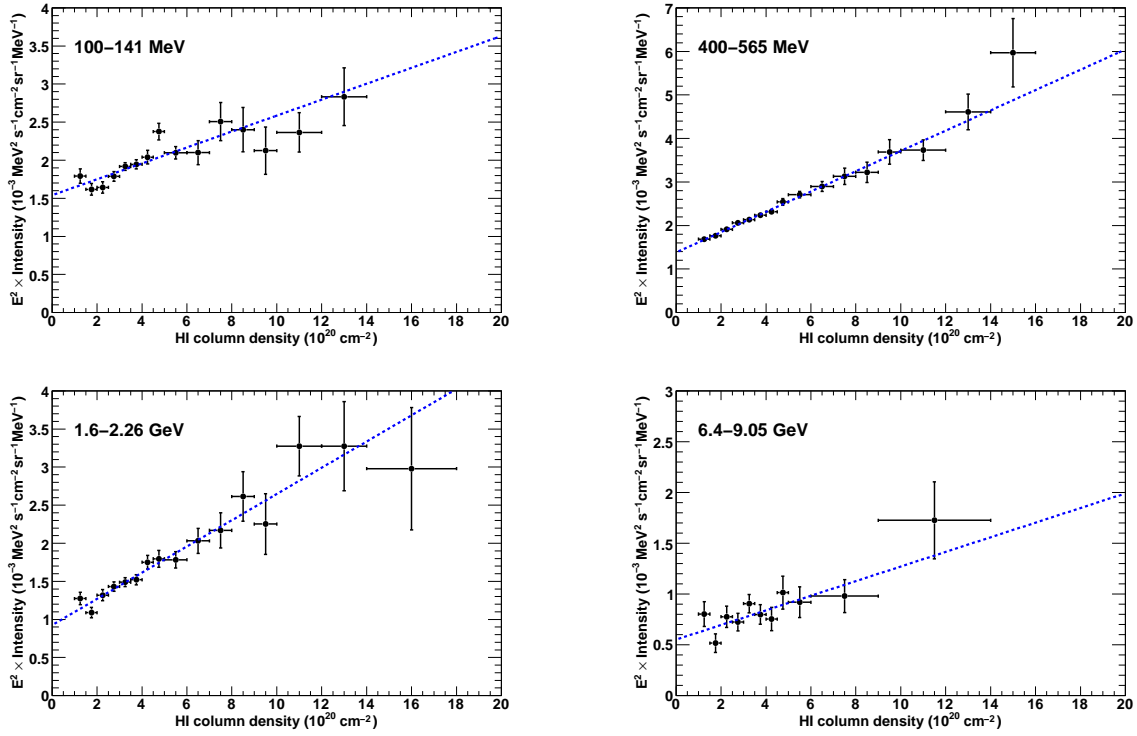


Fig. 4.— Correlation of the (IC and point-sources subtracted)  $\gamma$ -ray intensities and the HI column densities in four representative bands. The map of  $N(\text{HI})$  (Figure 3) is convolved with the LAT PSF of the corresponding energy range. The horizontal and vertical error bars indicate the ranges of the column density and the  $1 \sigma$  statistical errors, respectively. Data in high energy range (above 1 GeV) are rebinned to have more than 10  $\gamma$ -ray counts in each bin.

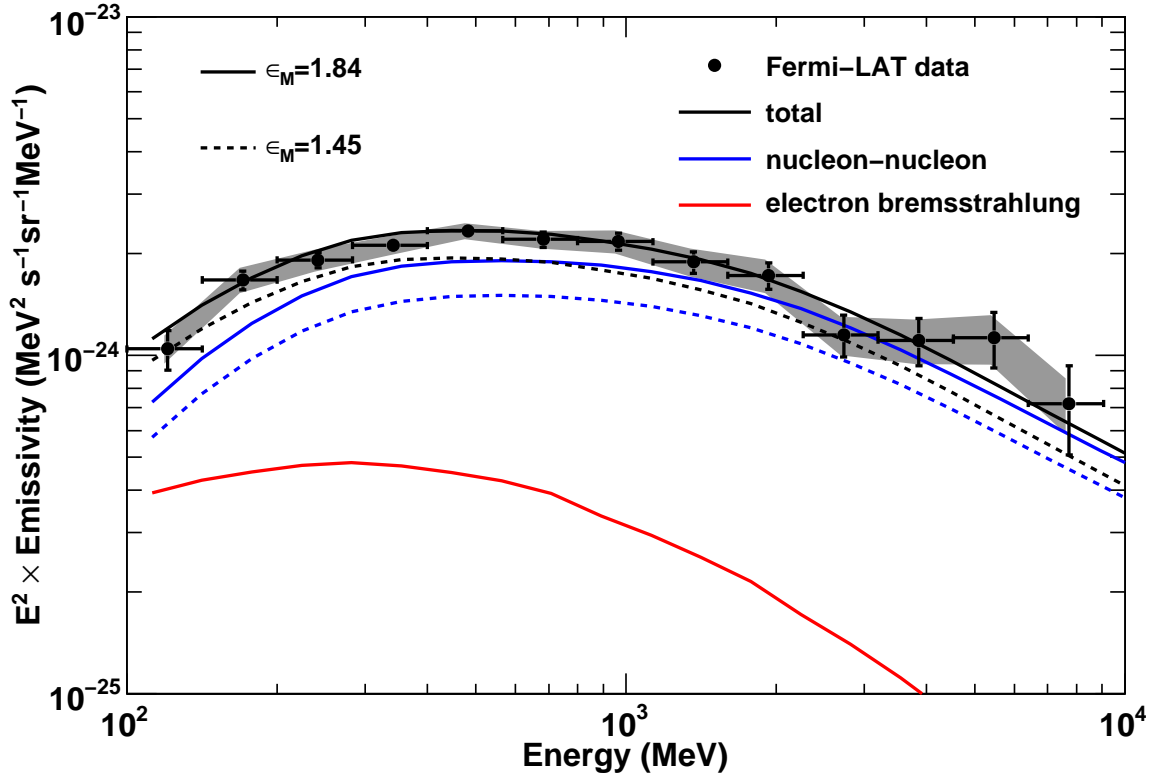


Fig. 5.— Differential  $\gamma$ -ray emissivity from the local atomic hydrogen gas compared with the calculated  $\gamma$ -ray production. The horizontal and vertical error bars indicate the energy ranges and  $1\sigma$  statistical errors, respectively. The assumed interstellar proton, electron and positron spectra are shown in Figure 6. Estimated systematic errors of the LAT data are indicated by the shaded area. A nucleus enhancement factor  $\epsilon_M$  of 1.84 is assumed for the calculation of the  $\gamma$ -rays from nucleon-nucleon interactions. Dotted lines indicate the emissivities for the case of  $\epsilon_M = 1.45$ , the lowest values in the referenced literature.

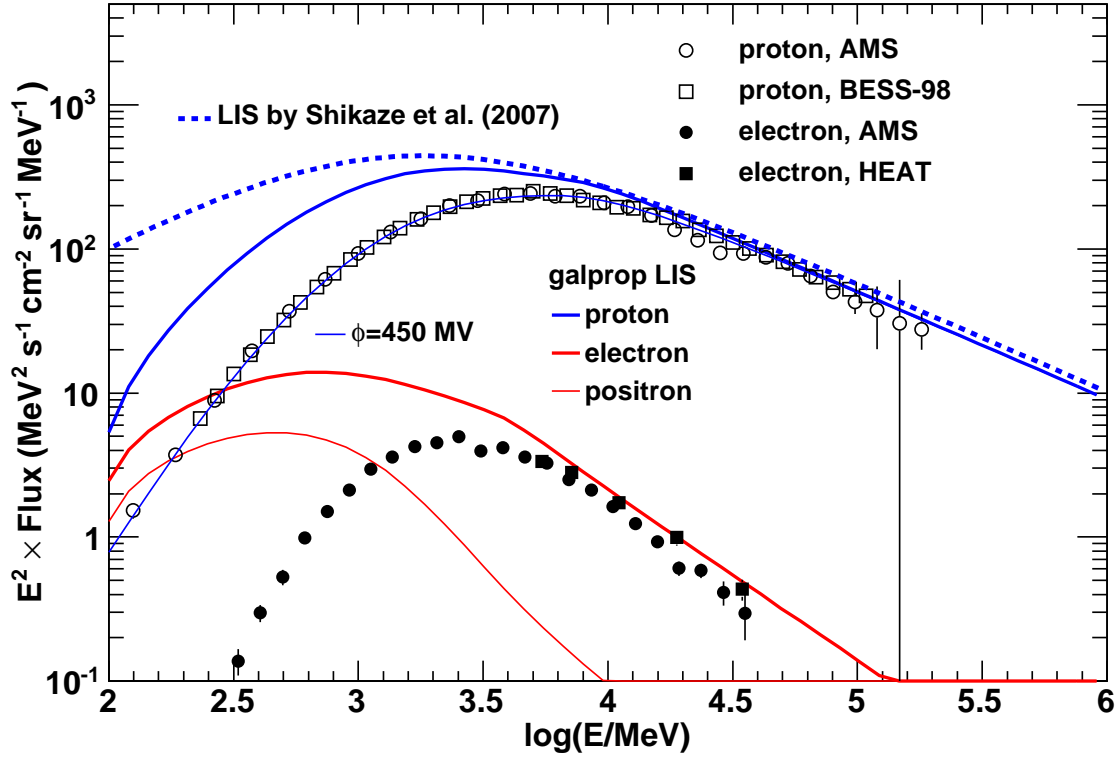


Fig. 6.— LIS of protons (thick blue line), electrons (thick red line) and positrons (thin red line) used to calculate the  $\gamma$ -ray emissivity model in Figure 5 with a compilation of direct measurements at the Earth; see Alcaraz et al. (2000a), Sanuki et al. (2000) and Shikaze et al. (2007) for proton data, and Alcaraz et al. (2000b) and Barwick et al. (1998) for electron data. Modulated spectrum with  $\phi = 450$  MV is given by thin blue line. The proton LIS adopted by Shikaze et al. (2007) is shown by dotted blue line.

Table 1. A summary of fit parameters with 1 Sigma statistical errors.

Energy GeV	Offset $10^{-4} \text{ MeV}^2 \text{ s}^{-1} \text{ cm}^{-2} \text{ sr}^{-1} \text{ MeV}^{-1}$	Slope $10^{-24} \text{ MeV}^2 \text{ s}^{-1} \text{ sr}^{-1} \text{ MeV}^{-1}$	$\chi^2/\text{dof}^{\text{a}}$	Data/Model counts <sup>b</sup>
0.10–0.14	$15.40 \pm 0.54$	$1.04 \pm 0.14$	21.90/13	11799/11678
0.14–0.20	$17.10 \pm 0.40$	$1.67 \pm 0.10$	18.12/14	27891/27738
0.20–0.28	$16.70 \pm 0.36$	$1.91 \pm 0.09$	13.47/14	31718/31564
0.28–0.40	$15.83 \pm 0.36$	$2.11 \pm 0.10$	16.92/14	28987/28850
0.40–0.56	$13.81 \pm 0.39$	$2.33 \pm 0.10$	6.65/14	22718/22073
0.56–0.80	$12.57 \pm 0.41$	$2.20 \pm 0.11$	16.17/15	16137/16063
0.80–1.13	$11.44 \pm 0.44$	$2.17 \pm 0.12$	12.26/15	11421/11368
1.13–1.60	$10.23 \pm 0.49$	$1.88 \pm 0.13$	9.06/14	7364/7327
1.60–2.26	$9.25 \pm 0.54$	$1.72 \pm 0.15$	13.16/14	4765/4733
2.26–3.20	$8.44 \pm 0.58$	$1.15 \pm 0.16$	10.56/12	2764/2747
3.20–4.53	$7.12 \pm 0.64$	$1.10 \pm 0.17$	15.07/11	1733/1712
4.53–6.40	$6.44 \pm 0.75$	$1.12 \pm 0.21$	11.35/11	1158/1144
6.40–9.05	$5.51 \pm 0.77$	$0.71 \pm 0.21$	9.92/9	678/664

<sup>a</sup>Degree of freedom

<sup>b</sup>Data and model total counts after masking point sources with circular regions of  $1^\circ$  radius. We believe that the small ( $\leq 1\%$ ) excesses of the data counts over the model counts are due to unresolved point sources or interstellar matter not traced by 21 cm line surveys.